Composite spin crystal phase in antiferromagnetic chiral magnets

S. A. Osorio,[1,2] H. D. Rosales,[1,2] M. B. Sturla,[1,2] and D. C. Cabra[1,2,3]
[1]*IFLP, UNLP, CONICET, Facultad de Ciencias Exactas, C.C. 67, 1900 La Plata, Argentina*
[2]*Departamento de Física, FCE, UNLP, 1900 La Plata, Argentina*
[3]*Abdus Salam International Centre for Theoretical Physics, Associate Scheme, Strada Costiera 11, 34151, Trieste, Italy*
(Received 7 December 2016; revised manuscript received 31 May 2017; published 6 July 2017)

We study the classical antiferromagnetic Heisenberg model on the triangular lattice with Dzyaloshinskii-Moriya interactions in a magnetic field. We focus in particular on the emergence of a composite spin crystal phase, dubbed an antiferromagnetic skyrmion lattice, that was recently observed for intermediate fields. This complex phase can be made up from three interpenetrated skyrmion lattices, one for each sublattice of the original triangular one. Following these recent numerical results, in this paper we explicitly construct the low-energy effective action that reproduces the correct phenomenology and could serve as a starting point to study the coupling to charge carriers, lattice vibrations, structural disorder, and transport phenomena.

DOI: 10.1103/PhysRevB.96.024404

I. INTRODUCTION

Antiferromagnets have been the focus of an enormous amount of work, mainly since the suggestion that they could be at the origin of the pairing mechanism in high-T_c superconductors [1]. On the other hand, in some chiral magnets such as MnSi [2–8], $Fe_{1-x}Co_xSi$ [9–11], FeGe [12–15], and $Mn_{1-x}Fe_xGe$ [16], a new kind of complex magnetic structure has been observed. This new phase, known as skyrmion crystal, observed in some range of temperatures and magnetic fields, consists of a periodic arrangement of topologically protected magnetic textures that resemble the one proposed by Skyrme [17].

The existence of these topological nanosized spin structures in condensed matter, called magnetic skyrmions, has been well known for a long time. In the case of chiral magnets, a rigorous analysis of isolated skyrmions was carried out in Refs. [18–20] (see [21]). Skyrmions also appear in systems like liquid crystals [22], quantum Hall ferromagnets [23], Bose condensates [24], etc.

The potential technological applications of this phase of chiral magnets are numerous. Among other things, the possibility of driving the motion of the magnetic skyrmions with ultralow current densities, an anomalous Hall effect, and the observed multiferroic behavior makes these systems particularly interesting for applications to processing devices and information storage, in particular racetrack memory devices [25,26]. On the other hand, the existence of high-frequency periodic excitations of the skyrmion lattice phase makes them promising candidates for nanoscale microwave resonators [27].

The underlying mechanism responsible for this structure seems to be an antisymmetric spin-orbit interaction, known as the Dzyaloshinskii-Moriya (DM) interaction [28,29]. In generic noncentrosymmetric magnetic crystals a DM interaction can stabilize a skyrmion crystal phase (SkX). The existence of these topologically protected structures in chiral magnets was theoretically predicted in [18,30–32]. Later, Yi *et al.* [33] showed using Monte Carlo simulations that a classical ferromagnetic spin system with DM interaction supports, in a given region of the parameter space, skyrmion lattice structures.

Han *et al.* [34] have proven that a nonlinear σ model plus a continuous version of the DM interaction in a magnetic field, proposed as the low-energy Hamiltonian of these chiral magnets, reproduces the observed phenomenology. Bogdanov and Yablonskii [35] have shown the stability of a skyrmion lattice in a large group of easy-axis bipartite antiferromagnetic systems. In a recent work [36], a detailed Monte Carlo simulation has shown the existence of an exotic magnetic phase on a triangular antiferromagnetic lattice in the presence of a DM interaction and for a certain window in the external magnetic field. This exotic phase, named AF-SkX, consists of a periodic arrangement which, observed by sublattice, resembles a ferromagnetic skyrmion phase (FM-SkX). The complete picture then corresponds to the three FM-SkX intertwined (as seen in Fig. 4 below). Such a phase arises in a frustrated simple antiferromagnetic model which exhibits remarkable new features, so one question that arises naturally is whether this novel magnetic background could promote some kind of pairing mechanism between electrons moving on top of such a magnetic profile [37]. As a first step in this direction, we identify and study in detail a simple low-energy effective description that reproduces the correct spin phenomenology and could serve as a first step to analyze the coupling between localized spins and conduction-electron spin, which could, in turn, give rise to interesting electron-transport phenomena [38]. For this purpose, based on a combined analysis using a variational approach and large-scale Monte Carlo simulations, we get quantitative predictions for the existence, the location, and the sizes of the AF-SkX phase induced by an external magnetic field.

The rest of this paper is organized as follows. In Sec. II we present the microscopic Hamiltonian and construct the continuous low-energy description. In Sec. III we propose variational *Ansätze* for the different phases that we expect from the numerical simulation results [36]. In Sec. IV we present the phase diagram of the continuous model obtained with these variational *Ansätze*. We find a rich low-temperature behavior of the system as the magnetic field is varied, recovering all the previously observed phases. The system goes from a helical phase (HL) at low fields to an antiferromagnetic skyrmion lattice phase (AF-SkX) for larger values of the field, and then,

before the ferromagnetic saturated phase (FM), there seems to be an intermediate phase, which we call the sublattice-uniform (SU) phase, which is described below. All our analytical predictions are supported by Monte Carlo (MC) simulations of the microscopic Hamiltonian. We conclude in Sec. V with a summary and discussion of our results.

II. MICROSCOPIC HAMILTONIAN AND CONTINUOUS LIMIT

We begin with the classical spin Hamiltonian in the two-dimensional triangular lattice (Fig. 1) given by

$$\mathcal{H} = \sum_{\langle \mathbf{r}\mathbf{r}'\rangle} [J\, \mathbf{S}_{\mathbf{r}} \cdot \mathbf{S}_{\mathbf{r}'} + \mathbf{D}_{\mathbf{r}\mathbf{r}'} \cdot (\mathbf{S}_{\mathbf{r}} \times \mathbf{S}_{\mathbf{r}'})] - \mathbf{B} \cdot \sum_{\mathbf{r}} \mathbf{S}_{\mathbf{r}}, \quad (1)$$

where $J > 0$ is the antiferromagnetic exchange constant, vectors $\mathbf{D}_{\mathbf{r}\mathbf{r}'}$ describe the antisymmetric (bulk) DM interaction ($\mathbf{D}_{\mathbf{r}\mathbf{r}'} \equiv -\mathbf{D}_{\mathbf{r}'\mathbf{r}}$) that stabilizes the AF-SkX phase recently described in Ref. [36] under an external magnetic field $\mathbf{B} = B\,\hat{z}$, and $\langle \mathbf{r}\mathbf{r}'\rangle$ indicates nearest neighbors (NN).

With the aim to obtain the continuous limit, it is more convenient to rewrite the previous Hamiltonian as a sum of plaquette Hamiltonians $\mathcal{H} = \sum_{\mathbf{r}} H_{\mathbf{r}}$, where $\mathbf{r}$ is the plaquette label. This procedure allows us to write the Hamiltonian density $H_{\mathbf{r}}$ in a symmetric way in terms of two indices i, j which denote the sublattices i and j (which from now on will be called the flavor index) and an index k denoting which neighbor of sublattice j we are considering [39] (see Fig. 1). Indices i, j, and k run from 1 to 3. From now on the $\mathbf{r}$ dependence of $H_{\mathbf{r}}$ (and the terms included in $H_{\mathbf{r}}$) and in the spin variables $\mathbf{S}_j$ is suppressed to simplify the notation, i.e., $H_{\mathbf{r}} \to H$, $\mathbf{S}_i(\mathbf{r}) \to \mathbf{S}_i$. The plaquette Hamiltonian density H reads

$$\begin{aligned} H &= H_E + H_{\rm DM} + H_z, \\ H_E &= \frac{J}{6} \sum_i \sum_{j\neq i} \sum_k \mathbf{S}_i \cdot \mathbf{S}_j^{(k)}, \\ H_{\rm DM} &= \frac{1}{6} \sum_i \sum_{j\neq i} \sum_k \mathbf{D}_{ij}^{(k)} \cdot \left(\mathbf{S}_i \times \mathbf{S}_j^{(k)}\right), \\ H_Z &= -\frac{1}{3} \sum_i \mathbf{B} \cdot \mathbf{S}_i. \end{aligned} \quad (2)$$

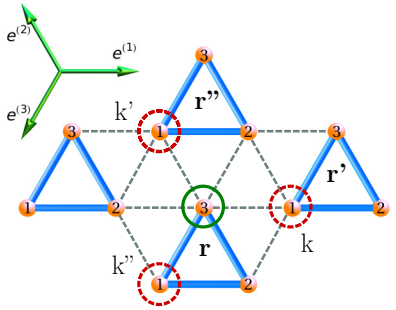

FIG. 1. Triangular lattice: $\mathbf{r}, \mathbf{r}', \mathbf{r}''$ indicate the plaquettes involved in a given term of the Hamiltonian density. As an example, the sublattice, labeled 3 (inside the green circle), in the plaquette in $\mathbf{r}$ has three first neighbors, denoted 1 (each one inside a red dashed circle) and indicated by labels k, k′ and k″. The bond director vectors are shown in the top left.

Assuming that each spin flavor varies slowly, an approximation that holds near both the ferromagnetic and antiferromagnetic orders, we can describe the continuum limit of each spin flavor by a smooth field configuration. Under such an assumption we can expand the value of the spin field $\mathbf{S}_j^{(k)}$ at site j around the position of the spin $\mathbf{S}_i$ as follows:

$$\mathbf{S}_j^k = \mathbf{S}_j + a\left[\mathbf{e}_{ij}^{(k)} \cdot \nabla\right]\mathbf{S}_j + \frac{a^2}{2}\left[\mathbf{e}_{ij}^{(k)} \cdot \nabla\right]^2 \mathbf{S}_j + O(a^3), \quad (3)$$

where a is the nearest-neighbor distance and $\mathbf{e}_{ij}^{(k)} = -\mathrm{sgn}[P(ij)]\mathbf{e}^{(k)}$, where $P(ij)$ is the permutation $(123) \to (ijl)$, with $\mathbf{e}^{(1)} = (1,0)$, $\mathbf{e}^{(2)} = (-\frac{1}{2}, \frac{\sqrt{3}}{2})$, $\mathbf{e}^{(3)} = (-\frac{1}{2}, -\frac{\sqrt{3}}{2})$ being the bond directors (see Fig. 1).

Performing a gradient expansion, the exchange Hamiltonian density up to second order in a reads

$$H_E = J \sum_i \sum_{j\neq i} \left(\frac{a^2}{8} \mathbf{S}_i \nabla^2 \mathbf{S}_j - \frac{1}{2} \mathbf{S}_i \cdot \mathbf{S}_j\right) + \text{const.} \quad (4)$$

The next term in Eq. (2) corresponds to the DM Hamiltonian density $H_{\rm DM}$. Let us define a cyclic DM vector $\mathbf{D}_{ij}^{(k)} = D\ \mathbf{e}_{ij}^{(k)}$ as in Ref. [36]. Using the gradient expansion (3), $H_{\rm DM}$, up to second order in a, becomes

$$\begin{aligned} H_{\rm DM} = \frac{1}{6} \sum_i \sum_{j\neq i} \sum_k \Big\{ & \mathbf{D}_{ij}^{(k)} \cdot (\mathbf{S}_i \times \mathbf{S}_j) \\ & + a\, \mathbf{D}_{ij}^{(k)} \cdot \left[\mathbf{S}_i \times \left(\mathbf{e}_{ij}^{(k)} . \nabla\right)\mathbf{S}_j\right] \\ & + \frac{a^2}{2} \mathbf{D}_{ij}^{(k)} \cdot \left[\mathbf{S}_i \times \left(\mathbf{e}_{ij}^{(k)} \cdot \nabla\right)^2 \mathbf{S}_j\right] \Big\}. \end{aligned} \quad (5)$$

The first term on the right side in (5) vanishes because $\sum_k \mathbf{e}_{ij}^{(k)} = 0$. Using the definitions of $\mathbf{D}_{ij}^{(k)}$ and $\mathbf{e}_{ij}^{(k)}$, the second term reads

$$\begin{aligned} & \frac{a}{6} \sum_i \sum_{j\neq i} \sum_k \mathbf{D}_{ij}^{(k)} \cdot \left[\mathbf{S}_i \times \left(\mathbf{e}_{ij}^{(k)} \cdot \nabla\right)\mathbf{S}_j\right] \\ & \quad = -\frac{aD}{4} \sum_i \sum_{j\neq i} \mathbf{S}_i \cdot (\nabla \times \mathbf{S}_j). \end{aligned}$$

Finally, the last term in (5) vanishes due to the antisymmetry of the DM coupling ($\mathbf{D}_{\mathbf{r}\mathbf{r}'} \equiv -\mathbf{D}_{\mathbf{r}'\mathbf{r}}$). Hence, the complete DM Hamiltonian density reads

$$H_{\rm DM} = -\frac{aD}{4} \sum_i \sum_{j\neq i} \mathbf{S}_i \cdot (\nabla \times \mathbf{S}_j). \quad (6)$$

Putting all the pieces together, we can write the complete Hamiltonian density H for an antiferromagnetic triangular chiral magnet in the continuous limit as

$$\begin{aligned} H = J \sum_{i,j\neq i} & \frac{1}{2} \mathbf{S}_i \cdot \mathbf{S}_j + \frac{a^2}{8} \mathbf{S}_i \nabla^2 \mathbf{S}_j - \frac{aD}{4J} \mathbf{S}_i \cdot (\nabla \times \mathbf{S}_j) \\ & - \frac{1}{3} \sum_i \mathbf{B} \cdot \mathbf{S}_i. \end{aligned} \quad (7)$$

The equations of motion of the previous Hamiltonian are nonlinear and fairly difficult to solve analytically. Instead, we study the Hamiltonian density proposing different families of *Ansätze*. In order to gain some intuition on the possible

expressions we rewrite (7) by introducing a nonindependent variable $M = \sum_i \mathbf{S}_i$, the plaquette magnetization. After some trivial algebraic manipulations Eq. (7) can be recast in the following form:

$$H = H_M + \sum_{i=1}^{3} H_i,$$
$$H_M = \frac{J}{2}(\mathbf{M}^2 - 3) + a^2\frac{J}{8}\mathbf{M}\cdot\nabla^2\mathbf{M} - \frac{aD}{4}\mathbf{M}\cdot(\nabla\times\mathbf{M}), \quad (8)$$
$$H_i = -a^2\frac{J}{8}\mathbf{S}_i\nabla^2\mathbf{S}_i + \frac{aD}{4}\mathbf{S}_i\cdot(\nabla\times\mathbf{S}_i) - \frac{1}{3}\mathbf{B}\cdot\mathbf{S}_i.$$

Some remarks are in order. We notice that the Hamiltonian density has been separated into four pieces. The first piece corresponds to a Hamiltonian density H_M for the plaquette magnetization, while the rest correspond to three copies of the same Hamiltonian density H_i, one for each flavor. Each of these H_i has exactly the form of the *ferromagnetic* nonlinear σ model studied by Han *et al.* [34] for chiral magnets. This is a crucial observation that, together with the knowledge of the finite-temperature phases of the system [36], motivates the *Ansätze* that we propose in the following section. We also call attention to the derivative term in the magnetization density that, at first sight, seems to lead to an energy unbounded from below. This is just an artifact of the introduction of the nonindependent variable $\mathbf{M}$. The Laplacian term in the magnetization density has its origin in the exchange interaction term

$$J\sum_i\sum_{j\neq i}\mathbf{S}_i\cdot\mathbf{S}_j = \frac{J}{2}(\mathbf{M}^2 - 3) + a^2\frac{J}{8}\mathbf{M}\cdot\nabla^2\mathbf{M} - a^2\frac{J}{8}\sum_i\mathbf{S}_i\nabla^2\mathbf{S}_i, \quad (9)$$

and since the left-hand side of Eq. (9) is bounded from below, the right-hand side should be as well. This means that the eventual large contribution that could arise from the term $a^2\frac{J}{8}\mathbf{M}\cdot\nabla^2\mathbf{M}$ will be compensated by the term $-a^2\frac{J}{8}\sum_i\mathbf{S}_i\nabla^2\mathbf{S}_i$. Hence, the full Hamiltonian remains bounded from below, as the original Hamiltonian. In fact, as will be explicitly described in the next section, the derivative terms of the magnetization in the solutions are orders of magnitude smaller than the rest of the terms that appear in the Hamiltonian density [Eq. (8)]

III. *ANSÄTZE* AND EFFECTIVE LOW-ENERGY HAMILTONIAN

The possibility to rewrite the continuum Hamiltonian as a sum of flavor Hamiltonian densities H_i plus a plaquette magnetization contribution H_M allows for an intuitive analysis. We mentioned in Sec. II that each flavor Hamiltonian is exactly the continuum model introduced by Han *et al.* [34] for two-dimensional ferromagnetic chiral magnets. Bogdanov *et al.* [18,30] and Han *et al.* [34] have shown that ferromagnetic chiral magnets admit nontrivial periodic magnetic textures known as skyrmion lattices (SkX). Hence, the presence of three almost independent H_i Hamiltonians in the continuum limit strongly suggests the possibility of a similar kind of nontrivial SkX solution on each sublattice.

These three independent equivalent SkX solutions need to be arranged in such a way that their sum, $\mathbf{M}$, minimizes the corresponding magnetization Hamiltonian.

A. Skyrmion crystal *Ansatz*

The proposed approximate solution to one spin flavor Hamiltonian can be constructed as a superposition of three helical solutions with wave vectors $\mathbf{k}_\mu$ satisfying $\sum_\mu \mathbf{k}_\mu = \mathbf{0}$ ($\mu = 1,2,3$) in the plane of the sample with relative angles of $2\pi/3$ [40]. The approximate skyrmion lattice solution then reads

$$\mathbf{n}_{\mathrm{SkX}}(\mathbf{r}) = \frac{1}{n}\left\{I_{xy}\sum_\mu \sin\left(\frac{2\pi}{T}\mathbf{k}_\mu\cdot\mathbf{r} + \theta_\mu\right)\mathbf{e}_{xy,\mu} + \left[m_z + I_z\sum_\mu\cos\left(\frac{2\pi}{T}\mathbf{k}_\mu\cdot\mathbf{r} + \theta_\mu\right)\right]\mathbf{e}_z\right\}, \quad (10)$$

where T is the period of each helix; n fixes the appropriate normalization $|\mathbf{n}_{\mathrm{SkX}}| = 1$, which restricts the values of the amplitudes I_{xy} (in plane) and I_z (perpendicular to the xy plane) and the homogeneous contribution to the magnetization in the z direction m_z. Here $\mathbf{e}_{xy,\mu}$ are arbitrary unit vectors lying on the xy plane satisfying $\sum_\mu \mathbf{e}_{xy,\mu} = \mathbf{0}$, while the phases θ_μ satisfy $\cos(\theta_1 + \theta_2 + \theta_3) = -1$ [40].

The helix period T can be determined as a function of I_{xy}, I_z, and m_z by energy-scale analysis (see the Appendix) and is related to the skyrmion lattice parameter R_{SkX} (the distance between skyrmion centers) through the equation $R_{\mathrm{SkX}} = \frac{2T}{\sqrt{3}}$.

Now, the proposed *Ansatz* for the full solution reads

$$\mathbf{S}_1(\mathbf{r}) = \mathbf{n}_{\mathrm{SkX}}(\mathbf{r}),\ \ \mathbf{S}_2(\mathbf{r}) = \mathbf{n}_{\mathrm{SkX}}(\mathbf{r} + \mathbf{T}_1),$$
$$\mathbf{S}_3(\mathbf{r}) = \mathbf{n}_{\mathrm{SkX}}(\mathbf{r} + \mathbf{T}_2), \quad (11)$$

where $\mathbf{T}_1, \mathbf{T}_2$ are arbitrary translations in the xy plane.

B. Helical *Ansatz*

In the helical phase, the spin structure is a special case of the *Ansatz* (10) and consists of three interpenetrating spirals on each sublattice, as in Eq. (11), but with a single-$\mathbf{k}_{\mu_0}$ mode,

$$\mathbf{n}_H(\mathbf{r}) = \frac{1}{n}\left\{I_{xy}\sin\left(\frac{2\pi}{T}\mathbf{k}_{\mu_0}\cdot\mathbf{r} + \theta\right)\mathbf{e}_{xy} + \left[m_z + I_z\cos\left(\frac{2\pi}{T}\mathbf{k}_{\mu_0}\cdot\mathbf{r} + \theta\right)\right]\mathbf{e}_z\right\}, \quad (12)$$

where again the constant n fixes the normalization $|\mathbf{n}_H| = 1$.

C. Uniform sublattice *Ansatz*

The magnetic phase diagram for the model defined by Eq. (1) with $D = 0$ has been discussed in [41,42]. At zero temperature and zero magnetic field the ground state is a planar configuration with spins arranged in a 120° structure described by the wave vector $k = (4\pi/3, 0)$. In a magnetic field the energy is minimized when the constraint

$$\mathbf{S}_1 + \mathbf{S}_2 + \mathbf{S}_3 = \mathbf{B}/(3J) \quad (13)$$

is fulfilled on each plaquette. This constraint persists up to the saturation field $B = 9J$, where the spins are fully polarized.

For $D \neq 0$ the previous discussion breaks down since the DM term stabilizes new configurations. However, it is worth noting that even for $D \neq 0$ there exist spin configurations in which the DM contribution cancels out. This is the case when the spin field on each sublattice is uniform. This is easily seen from our effective model since the DM term contains derivatives of the spin fields. If one goes back to the microscopic model, one can show that the sum of the interactions (through DM) of a specific spin with its six neighbors is zero for the present choice of the **D** vectors. Thus, for this kind of configuration, which we denote SU for "sublattice uniform" from now on, the constraint given by Eq. (13) is still valid, and this is an equilibrium state to be considered in the following discussion of the phase diagram.

The energy per plaquette of the states satisfying the constraint (13) is field dependent, independent of D, and is given by

$$E_{SU} = -\frac{B^2}{18J} - J\frac{3}{2}. \tag{14}$$

Finally, at the saturation the energy per plaquette of the ferromagnetic state (for $B > 9J$) is

$$E_{\mathrm{FM}} = 3J - B. \tag{15}$$

Now that we have described the *Ansätze* under which we will study the Hamiltonian, we are in the position to compare the values of the terms that include derivatives of **M** to the rest of the terms included in the Hamiltonian density (8). First, let us analyze these terms in the helix phase. In this case, the plaquette magnetization corresponds to a superposition of three helical waves, each one given by Eq. (12), separated (in space) by a translation in the direction of propagation. In the case where the distance between peaks is uniform (i.e., the phase difference of each cosine is $2\pi/3$) it is straightforward to see from the *Ansatz* (12) that **M** will show small spatial variations: $\mathbf{M}(\mathbf{r}) \approx \mathbf{M} = \text{const}$. For the SkX phase, a similar analysis drives us to the same conclusion. These statements are confirmed by our numerical calculations performed for both *Ansätze* for different values of the coupling D and as a function of **B**. Our results show that the plaquette magnetization is almost constant, leading to the conclusion that the contribution of the Laplacian and curl terms in H_M are two orders of magnitude smaller than the rest of the terms present in the Hamiltonian density (8) (see Fig. 2). For this purpose we compare the four contributions (with spatial derivatives) of the total energy, namely, E_{nlsm}, E_{dm}, E_{Mnlsm}, and E_{Mdm}, where

$$E_{\mathrm{nlsm}} = -a^2\frac{J}{8}\sum_{\mathbf{r}}\sum_{i}\mathbf{S}_i\nabla^2\mathbf{S}_i, \tag{16}$$

$$E_{\mathrm{dm}} = \frac{aD}{4}\sum_{\mathbf{r}}\sum_{i}\mathbf{S}_i\cdot(\nabla\times\mathbf{S}_i), \tag{17}$$

$$E_{\mathrm{Mnlsm}} = a^2\frac{J}{8}\sum_{\mathbf{r}}\mathbf{M}\cdot\nabla^2\mathbf{M}, \tag{18}$$

$$E_{\mathrm{Mdm}} = -\frac{aD}{4}\sum_{\mathbf{r}}\mathbf{M}\cdot(\nabla\times\mathbf{M}). \tag{19}$$

In Fig. 2 we plot the ratios between the four terms (16)–(19), setting E_{dm} as the scale, for the case $D/J = 1/2$. We observe that in the HL and AF-SkX phases both $E_{\mathrm{Mnlsm}}/E_{\mathrm{dm}}$ and $E_{\mathrm{Mdm}}/E_{\mathrm{dm}}$ are negligible in almost all the field range, except for two narrow windows around the transition fields where the value of these ratios are smaller than 5×10^{-2}. In the homogeneous SU and FM phases all the terms with derivatives are zero. This behavior is repeated in the whole range that we have explored, $D/J < 1$, leading to the conclusion that the contributions of the Laplacian and curl terms in H_M are at least two orders of magnitude smaller than the rest of the terms present in the Hamiltonian.

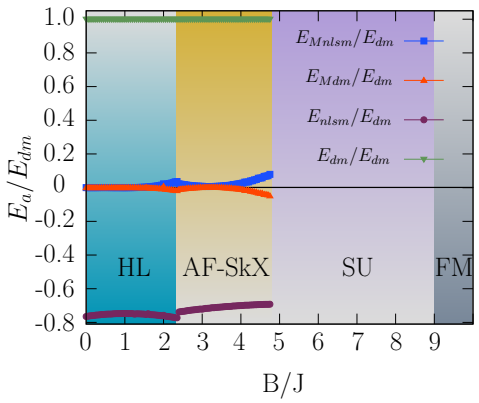

FIG. 2. Comparison between different contributions from the density Hamiltonian (8) for the case $D/J = 1/2$. We compare the four terms $E_a = \{E_{\mathrm{nlsm}}, E_{\mathrm{dm}}, E_{\mathrm{Mnlsm}}, E_{\mathrm{Mdm}}\}$ [see Eqs. (16)–(19)] using E_{dm} as a scale. In the HL and AF-SkX phases, the dominant terms are those coming from $\sum_i H_i$ in Eq. (8). All these terms are zero in the SU and FM (homogeneous) phases.

Monte Carlo simulations show that the spatial variation of the magnetization is small compared to the variation of the spin on each sublattice, confirming the observation made by the variational approach. Based on the previous analysis, we end up this section by proposing a simplified low-energy effective Hamiltonian that captures the low-energy physics of the antiferromagnetic chiral magnet given by Eq. (1).

D. Effective low-energy theory

From the previous discussion the effective Hamiltonian is given by

$$\begin{aligned} H^{\mathrm{eff}} &= \sum_{i=1}^{3} H_i + H_M^{\mathrm{eff}}, \\ H_i &= -a^2\frac{J}{8}\mathbf{S}_i\nabla^2\mathbf{S}_i + \frac{aD}{4}\mathbf{S}_i\cdot(\nabla\times\mathbf{S}_i) - \frac{1}{3}\mathbf{B}\cdot\mathbf{S}_i, \\ H_M^{\mathrm{eff}} &= \frac{J}{2}(\mathbf{M}^2 - 3), \end{aligned} \tag{20}$$

where H_M^{eff} corresponds to the simplified version of H_M in (8), which we have shown captures all the essential details of the phase diagram.

It is remarkable that this continuum effective Hamiltonian can be thought of as the sum of three Ginzburg-Landau effective actions (one for each flavor/sublattice) plus a term H_M^{eff} that couples them. From the first term of the sum one could expect, separately on each sublattice, the three well-known phases, HL, SkX and FM.

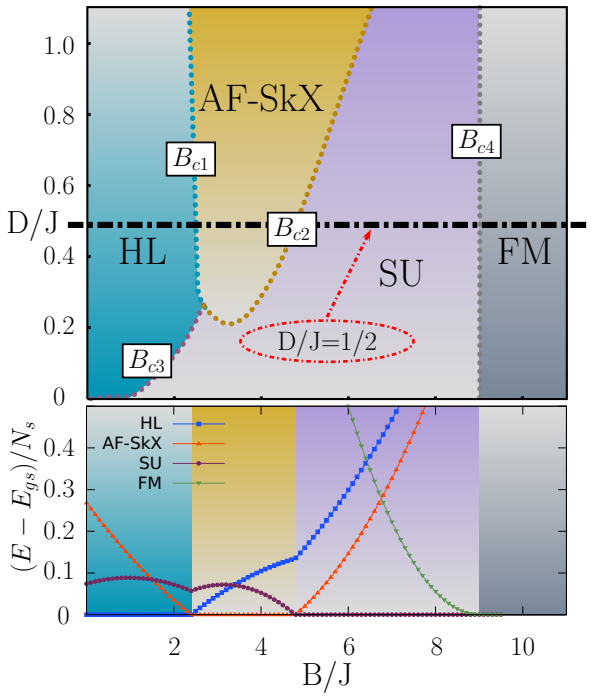

FIG. 3. Top: Phase diagram; dotted lines correspond to the boundaries between different phases labeled by the fields $B_{c1}, \ldots, B_{c4}$ (functions of D). Bottom: The energies ($E_{\text{phase}} - E_{\text{gs}}$) of the three states of a triangular antiferromagnetic chiral magnet with $D/J = 1/2$ as a function of the external magnetic field B. This example corresponds to the path indicated by the dashed black line in the phase diagram.

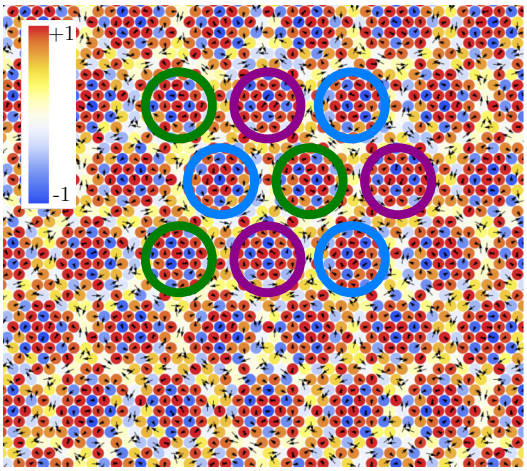

FIG. 4. Representative magnetic texture obtained by low-energy effective theory [Eq. (20)] and the variational *Ansatz* for $D/J = 1/2$ and $B/J = 3$. Arrows indicate the xy component of the spins, while the colored dots (from blue to red) indicate their z component. The circles (green, blue, and purple) indicate the positions of the skyrmion cores on each sublattice.

IV. RESULTS AND PHASE DIAGRAM

In this section we construct the full phase diagram of the Hamiltonian (20), paying particular attention to the appearance of the topological AF-SkX phase.

In the study of the phase diagram we consider four phases, namely, the HL and SkX phases with energies E_{HL} and E_{SkX}, respectively, together with the SU and FM phases presented in Sec. III. To find the minimum-energy configuration we fix the variational parameters in a self-consistent way by using the Nelder-Mead simplex method, which is one of the most used for direct optimization [43]. The procedure consists of introducing an initial guess for I_{xy} and m_z and determining variationally the values of $\mathbf{T_1}$ and $\mathbf{T_2}$ self-consistently. It turns out that $\mathbf{T_1}$ and $\mathbf{T_2}$ are related to the parameter T. We find that $\mathbf{T_2} = -\mathbf{T_1} = \frac{2T}{3}\hat{\mathbf{x}}$ for the skyrmion lattice, while for the helical phase $\mathbf{T_2} = -\mathbf{T_1} = \frac{T}{3}\hat{\mathbf{x}}$.

The minimization of the variational energies for the different phases leads to the phase diagram shown in the top panel of Fig. 3, where the boundaries of the phases result from level crossings as shown in the bottom panel of Fig. 3. As an example, in Fig. 4 we show a representative spin texture obtained by the variational *Ansatz* in the AF-SkX phase ($D/J = 1/2$ and $B/J = 3$). The colored circles in Fig. 4 indicate the cores of the skyrmion on each sublattice.

The main feature of this diagram is the presence of the four phases, namely, HL, AF-SkX, SU, and FM, in a wide region of $D - B$ ($D > 0$) space. However, there exists a critical value $D_c \approx 0.2$ for the skyrmion lattice to be stable. Below this value, the skyrmion lattice phase is excluded irrespective of the magnitude of the external field. The phase diagram for small fields is dominated by a helical phase with a wave vector lying in the plane. This phase starts at zero magnetic field $B = 0$ and extends to B_{c3} for $D < D_c$ and to B_{c1} for $D > D_c$ (see Fig. 3).

The phase diagram presents a wide region with a complex magnetic texture that is described by the superposition of three skyrmion lattices, one for each flavor. The region of the parameter space where this phase is stable is delimited by the curves B_{c1} and B_{c2}. From B_{c2} and B_{c3} up to the saturation field B_{c4} the SU phase is realized.

For the HL and AF-SkX phases, the optimized value of the period T shows a small linear dependence in the external field (the same for both phases as obtained by MC simulations [36]). In Fig. 5 we see that the mean period takes the same values for the HL state and for the AF-SkX state as $T(J/D) \simeq \frac{6.57J}{D} - 1.95$.

For $D/J = 1/2$, we get $T \approx 10.8 \pm 0.6$ (this value should be compared with the wavelength $T \approx 11.4$ of the HL and AF-SkX phases found in Ref. [36] obtained by numerical simulations of finite-size systems). We can define the radius of a skyrmion (in one sublattice) as the radius of the circumference of the contour defined by $n_z = 0$. In the inset in the top panel of Fig. 5 we show the skyrmion size as a function of the magnetic field. We observe that the behavior of the optimal skyrmion spacing as a function of the magnetic field varies very slowly in the region of the AF-SkX phase due to its topological stability. This behavior translates precisely in a wide range of stability of the AF-SkX phase in which the skyrmion number is fixed.

It is important here to review some of the basic facts concerning the behavior of skyrmion lattices in chiral ferromagnets and to compare them with the present results for antiferromagnetic systems. In chiral ferromagnetic systems two parameters are relevant in the characterization of the skyrmion structure. The first is the skyrmion core, which tends to decrease as the magnetic field grows [44], in order to

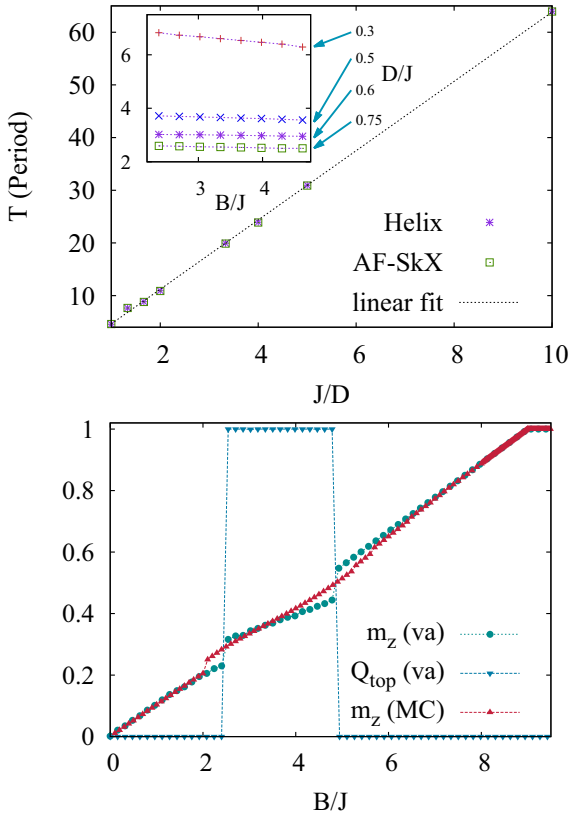

FIG. 5. Top: Variation of the period with J/D for SkX (green squares) and HL (purple stars). We used J/D instead of D/J to obtain a linear fit. Inset: The skyrmion radius as a function of the external magnetic field for several values of D/J. Bottom: Topological charge Q_{top} and magnetization m_z^T as a function of the magnetic field for $D = 0.5J$ and magnetization vs magnetic field B calculated by the variational *Ansatz* and by MC simulations.

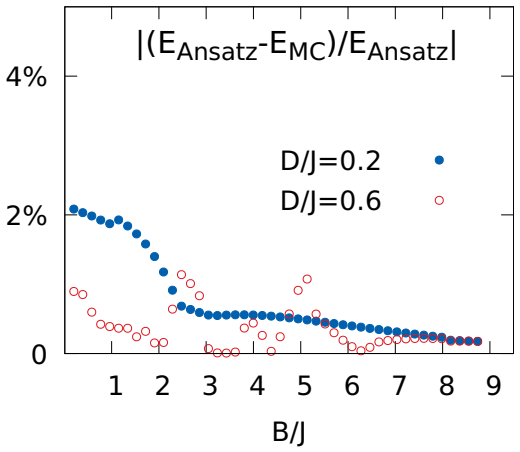

FIG. 6. Comparison of the results from the variational *Ansatz* and MC simulations for $D/J = 0.2$ and 0.6. We plot the relative error $|(E_{Ansatz} - E_{MC})/E_{Ansatz}|$ vs magnetic field (B/J) as an indicator of the good agreement between both approaches. The specific values of D/J were chosen as being representative of two possible paths as a function of the external field B: one that goes directly from the HL phase to the SU phase (0.2 case) and another in which the path goes through the AF-SkX phase (0.6).

increase the field polarized (FM) background. As shown in the top panel of Fig. 5, this behavior is present for the skyrmions in the antiferromagnetic system too. The second parameter is the skyrmion lattice period, which takes into account the distance between two adjacent skyrmions. In the ferromagnetic case the system goes from the SkX to the FM state, where a divergence of the skyrmion lattice period is observed [44]. This divergence takes place precisely at the boundary of the SkX-FM coexistence region (where the energy of the FM phase equals the energy of the SkX phase). In contrast, in the antiferromagnetic system, the transition occurs in a different way: the system goes from AF-SkX to the SU state and then to the FM phase as the magnetic field is increased. Then the system undergoes a phase transition to the SU phase before the skyrmion lattice period starts to grow.

In order to capture the topological character of the field configuration for each spin flavor we introduce the topological index Q_{top} and define the total (normalized) magnetization (z component):

$$Q_{\text{top}} = \frac{1}{4\pi} \int_{u.c.} \mathbf{n} \cdot (\partial_x \mathbf{n} \times \partial_y \mathbf{n})\, d^2 r, \tag{21}$$

$$m_z^T = \frac{1}{A_{u.c.}} \int_{u.c.} n_z\, d^2 r, \tag{22}$$

where the integration is performed in a unit cell of the magnetic texture with area $A_{u.c.}$ (see the Appendix).

In the bottom panel of Fig. 5 we show the behavior of the magnetization and the topological charge as a function of the magnetic field. We see that the helical phase corresponds to a trivial configuration with $Q_{\text{top}} = 0$, whereas in the SkX phase (triple-helix state) $Q_{\text{top}} = 1$ because each unit cell contains only one skyrmion. The magnetization curve reveals an almost linear growth up to the saturation field. However, we see two discontinuities, suggesting a first-order phase transition from HL to the AF-SkX phase and from AF-SkX to the SU phase.

In order to confirm the results from the variational analysis, we numerically examine the ground state of the model (1) using Monte Carlo simulations based on the standard heat-bath method combined with the overrelaxation method. We have implemented periodic boundary conditions for $N = 3600$ sites. A run at each magnetic field or temperature contains typically 0.1–1×10^6 Monte Carlo steps (MCSs) for the initial relaxation and twice as many MCSs during the calculation of mean values. In the bottom panel of Fig. 5 we compare magnetization vs magnetic field for the minimized variational solution and using MC simulations for $D/J = 1/2$. We observe qualitative agreement between both methods. However, the behavior of the magnetization differs when the system switches from one phase to another. This may be due to finite-size effects of the MC simulations and the fact that in the transition region, the variational solution does not include higher-order modes in $\mathbf{k}$. In Fig. 6 we compare the ground-state energy as a function of the magnetic field obtained from the minimization of the variational energies for the different phases and using MC simulations for two values of D/J. The excellent agreement between both results further supports the variational analysis of the continuous limit of the microscopic Hamiltonian given by Eq. (20).

V. DISCUSSION AND CONCLUSION

To summarize, we have constructed a low-energy theory describing the behavior of the Heisenberg model in the triangular lattice including Dzyaloshinskii-Moriya interactions and the magnetic field. Our low-energy effective theory given in Eq. (20), notwithstanding its simplicity, displays a plethora of phenomena of current interest in the context of topological magnetic phases. The effective theory obtained surprisingly consists of three independent Hamiltonian densities H_i similar to those found by Bogdanov *et al.* [18,30] and Han *et al.* [34] in the context of ferromagnetic systems. Each one of these admits nontrivial magnetic structures known as skyrmion lattices (SkX). In addition to these terms, there is a plaquette magnetization contribution H_M which couples the previous H_i. The low-energy theory predicts an AF-SkX crystal phase which consists of three interpenetrating SkX states as observed in numerical Monte Carlo simulations [36]. The low-energy effective Hamiltonian reproduces the correct spin phenomenology and could serve as a first step to analyze the coupling to charge degrees of freedom. In addition we numerically examined the low-temperature properties of the microscopic model using Monte Carlo simulations, showing very good agreement between both methods. This effective Hamiltonian could serve as a starting point to study the coupling to charge carriers, lattice vibrations, structural disorder, and transport phenomena. Once the effective action is obtained, one can envisage the inclusion of charge carriers, which would interact via Hund coupling to the magnetic background, and this could serve as a starting point to study transport phenomena. The coupling to lattice vibrations and structural disorder would enter through the standard deviation of the exchange couplings J_{ij}. Finally, the remarkable stability that presents the AF-SkX phase for a wide range of magnetic fields can have interesting consequences in the context of the anomalous Hall effect.

ACKNOWLEDGMENTS

The authors especially thank P. Pujol, N. Grandi, and G. Rossini for fruitful discussions. This work was partially supported by CONICET (PIP 0747) and ANPCyT (PICT 2012-1724).

APPENDIX: ENERGY-SCALE ANALYSIS

The magnetic textures considered in Sec. III, namely, helix and AF-SkX, are periodic configurations in the x and y directions with periods αT and βT, respectively, with α,β fixed by the symmetry of the texture (for the helix $\alpha = \beta = 1$, and for AF-SkX $\alpha = 1$ and $\beta = 2/\sqrt{3}$). This allows us to calculate the total energy as the energy of a cell (of area $A_{u.c.} = \alpha\beta T^2$) times the number of cells, $L^2/(\alpha\beta T^2)$, in the sample. In addition, we separate different contributions in the energy density according to the order of spatial derivatives. With all this, the total energy can be written as

$$E(T,I_{xy},I_z,m_z) = \frac{L^2}{\alpha\beta T^2}\sum_{i=0}^{2} E_i(T,I_{xy},I_z,m_z), \tag{A1}$$

with

$$E_i(T,I_{xy},I_z,m_z) = \int_0^{\alpha T} dx \int_0^{\beta T} dy\, \mathcal{E}_i(T,I_{xy},I_z,m_z), \tag{A2}$$

where $\mathcal{E}_i(T,I_{xy},I_z,m_z)$ denotes the energy density containing ith-order derivatives. We can rewrite the different terms using their properties under scale transformations ($\mathbf{r} \to \mathbf{r}' = \mathbf{r}/T$). We can separate the dependence in T as

$$\begin{aligned} E_i(T,I_{xy},I_z,m_z) &= \int_0^{\alpha T} dx \int_0^{\beta T} dy\, \mathcal{E}_i(T,I_{xy},I_z,m_z) \\ &= T^{2-i}\int_0^{\alpha} dx' \int_0^{\beta} dy'\, \mathcal{E}_i(1,I_{xy},I_z,m_z) \\ &= T^{2-i} E_i(1,I_{xy},I_z,m_z) \end{aligned}$$

and write the energy of the sample as

$$E(T,I_{xy},I_z,m_z) = \frac{L^2}{\alpha\beta}\left[\frac{E_2}{T^2} + \frac{E_1}{T} + E_0\right].$$

This shows that all the dependence on the variable T can be cast as power-law prefactors.

[1] P. W. Anderson, Science **235**, 1196 (1987).
[2] S. Mühlbauer, B. Binz, F. Jonietz, C. Pfleiderer, A. Rosch, A. Neubauer, R. Georgii, and P. Böni, Science **323**, 915 (2009).
[3] Y. Ishikawa, K. Tajima, D. Bloch, and M. Roth, Solid State Commun. **19**, 525 (1976).
[4] Y. Ishikawa and M. Arai, J. Phys. Soc. Jpn. **53**, 2726 (1984).
[5] S. V. Grigoriev, V. A. Dyadkin, E. V. Moskvin, D. Lamago, Th. Wolf, H. Eckerlebe, and S. V. Maleyev, Phys. Rev. B **79**, 144417 (2009).
[6] B. Lebech, P. Harris, J. S. Pedersen, K. Mortensen, C. Gregory, N. Bernhoeft, M. Jermy, and S. Brown, J. Magn. Magn. Mater. **140–144**, 119 (1995).
[7] C. Pfleiderer, D. Reznik, L. Pintschovius, H. v. Löhneysen, M. Garst, and A. Rosch, Nature (London) **427**, 227 (2004).
[8] M. Janoschek, M. Garst, A. Bauer, P. Krautscheid, R. Georgii, P. Böni, and C. Pfleiderer, Phys. Rev. B **87**, 134407 (2013).
[9] J. Beille, J. Voiron, and M. Roth, Solid State Commun. **47**, 399 (1983).
[10] S. V. Grigoriev, V. A. Dyadkin, D. Menzel, J. Schoenes, Yu. O. Chetverikov, A. I. Okorokov, H. Eckerlebe, and S. V. Maleyev, Phys. Rev. B **76**, 224424 (2007).
[11] Y. Onose, N. Takeshita, C. Terakura, H. Takagi, and Y. Tokura, Phys. Rev. B **72**, 224431 (2005).
[12] B. Lebech, J. Bernhard, and T. Freltoft, J. Phys. Condens. Matter **1**, 6105 (1989).
[13] M. Uchida, N. Nagaosa, J. P. He, Y. Kaneko, S. Iguchi, Y. Matsui, and Y. Tokura, Phys. Rev. B **77**, 184402 (2008).
[14] X. Yu, N. Kanazawa, Y. Onose, K. Kimoto, W. Zhang, S. Ishiwata, Y. Matsui, and Y. Tokura, Nat. Mater. **10**, 106 (2011).
[15] H. Wilhelm, M. Baenitz, M. Schmidt, U. K. Rößler, A. A. Leonov, and A. N. Bogdanov, Phys. Rev. Lett. **107**, 127203 (2011).

[16] K. Shibata, X. Yu, T. Hara, D. Morikawa, N. Kanazawa, K. Kimoto, S. Ishiwata, Y. Matsui, and Y. Tokura, Nat. Nanotechnol. **8**, 723 (2013).
[17] T. H. R. Skyrme, Nucl. Phys. **31**, 556 (1962).
[18] A. Bogdanov and A. Hubert, J. Magn. Magn. Mater. **138**, 255 (1994).
[19] A. Bogdanov and A. Hubert, Phys. Status Solidi B **186**, 527 (1994).
[20] A. Bogdanov and A. Hubert, J. Magn. Magn. Mater. **195**, 182 (1999).
[21] In Ref. [36] we involuntarily missed some important earlier references on the study of skyrmions [35,18,19,20], which have been included here. We thank A. Bogdanov for pointing these references out to us.
[22] D. C. Wright and N. D. Mermin, Rev. Mod. Phys. **61**, 385 (1989).
[23] S. L. Sondhi, A. Karlhede, S. A. Kivelson, and E. H. Rezayi, Phys. Rev. B **47**, 16419 (1993).
[24] T.-L. Ho, Phys. Rev. Lett. **81**, 742 (1998).
[25] J. Sampaio, V. Cros, S. Rohart, A. Thiaville, and A. Fert, Nat. Nanotechnol. **8**, 839 (2013).
[26] R. Tomasello, E. Martinez, R. Zivieri, L. Torres, M. Carpentieri, and G. Finocchio, Sci. Rep. **4**, 6784 (2014).
[27] T. Schwarze, J. Waizner, M. Garst, A. Bauer, I. Stasinopoulos, H. Berger, C. Pfleiderer, and D. Grundler, Nat. Mater. **14**, 478 (2015).
[28] I. Dzyaloshinsky, J. Phys. Chem. Solids **4**, 241 (1958).
[29] T. Moriya, Phys. Rev. Lett. **4**, 228 (1960).
[30] A. Bogdanov and D. Yablonskii, Zh. Eksp. Teor. Fiz. **95**, 178 (1989) [Sov. Phys. JETP **68**, 101 (1989)].
[31] U. Rößler, A. Bogdanov, and C. Pfleiderer, Nature (London) **442**, 797 (2006).
[32] U. K. Rößler, A. A. Leonov, and A. N. Bogdanov, J. Phys. Conf. Ser. **303**, 012105 (2011).
[33] S. D. Yi, S. Onoda, N. Nagaosa, and J. H. Han, Phys. Rev. B **80**, 054416 (2009).
[34] J. H. Han, J. Zang, Z. Yang, J.-H. Park, and N. Nagaosa, Phys. Rev. B **82**, 094429 (2010).
[35] A. Bogdanov and D. Yablonskii, Zh. Eksp. Teor. Fiz. **96**, 253 (1989) [Sov. Phys. JETP **69**, 142 (1989)].
[36] H. D. Rosales, D. C. Cabra, and P. Pujol, Phys. Rev. B **92**, 214439 (2015).
[37] G. Baskaran, arXiv:1108.3562.
[38] J. Zang, M. Mostovoy, J. H. Han, and N. Nagaosa, Phys. Rev. Lett. **107**, 136804 (2011).
[39] T. Dombre and N. Read, Phys. Rev. B **39**, 6797 (1989).
[40] T. Okubo, S. Chung, and H. Kawamura, Phys. Rev. Lett. **108**, 017206 (2012).
[41] M. V. Gvozdikova, P.-E. Melchy, and M. E. Zhitomirsky, J. Phys. Condens. Matter **23**, 164209 (2011).
[42] L. Seabra, T. Momoi, P. Sindzingre, and N. Shannon, Phys. Rev. B **84**, 214418 (2011).
[43] J. A. Nelder and R. Mead, Comput. J. **7**, 308 (1965).
[44] A. B. Butenko, A. A. Leonov, U. K. Rößler, and A. N. Bogdanov, Phys. Rev. B **82**, 052403 (2010).